

EXPERIMENTAL INVESTIGATION OF THE EFFECT OF VARIOUS WINGLET SHAPES ON THE TOTAL PRESSURE DISTRIBUTION BEHIND A WING

Mohammad Reza Soltani, Kaveh Ghorbanian, Mehdi Nazarinia
Department of Aerospace Engineering, P. O. Box: 11365-8639
Sharif University of Technology, Tehran, 14566, Iran

Keywords: *Winglets, Pressure Distribution, Tip Vortex, Winggrid, Turbulator*

Abstract

A series of low speed wind tunnel tests to investigate the effect of different winglet shapes and orientations on the flowfield of a swept wing were conducted. Both surface pressure and wake data at various angles of attack, $\alpha = -10$ to 15 degrees were measured. Further, the flowfield around the wing is visualized using tufts. Four types of winglet shapes, spiroid (forward and aft), blended and winggrid are used in this investigation. The wake profile behind the wing at various angles of attack with different winglets is measured, too. Furthermore, the effect of Turbulator strip on the wing upper surface is examined. Results are compared with conditions of no winglet. The results indicate that the presence of winglets change the flowfield over and around the wing significantly. The total pressure in the wake of the model varies drastically when the wing is equipped with winglets.

1 Introduction

From the beginning of aviation, designers are searching for methods and technologies to reduce the required fuel consumption of commercial aircraft. Wingtip devices aim the reduction of induced drag, which are responsible for 30-40% of the total drag of a transport-aircraft at long-range cruise condition and for considerably downgrading the climb performance of an aircraft. Winglets along tip tanks, raked wingtips, and aligned fans belong to this class of devices. During 1980s, NASA Dryden Flight Research Center was involved with general aviation research with the KC-135 aircraft. A winglet,

developed by Richard Whitcomb of the Langley Research Center, was tested on a KC-135A tanker loaned to NASA by the Air Force. The flight test showed that the winglets could increase the aircraft's range by as much as 7 percent at cruise speeds. The first application of NASA's winglet technology in industry was on General Aviation business jets, but winglets are now incorporated into most commercial and military transport jets, i.e., the Gulfstream III, IV, and V business jets, the Boeing 747-400, McDonnell Douglas MD-11 and Airbus A340, A330, A310-300, A321, airliners, the McDonnell Douglas C-17 military transport, and Embraer aircraft. In recent years, many modification kits are offered for installing winglets to aircrafts, which originally did not have them.

A close look at the drag breakdown of a typical civil transport aircraft (Fig.1), reveals that the skin friction and lift induced drag together represent more than 80% of the total drag and may offer the highest potential for drag reduction. The remaining components, while of no less importances represent only about 20%, of the total drag.

Induced drag is one of the major contributors (about 35%) of the total aircraft drag, Figure 1. Various research programs are concentrated on using wing tip devices to increase the effective span of the wing. Integrated winglet concept, with continuous evolution of the wing tip shape has been studied by several research centers worldwide. Among the various types studied, new concepts such as spiroid winglets seems to be the most promising ones [1], which is the focus of the present experimental work as well.

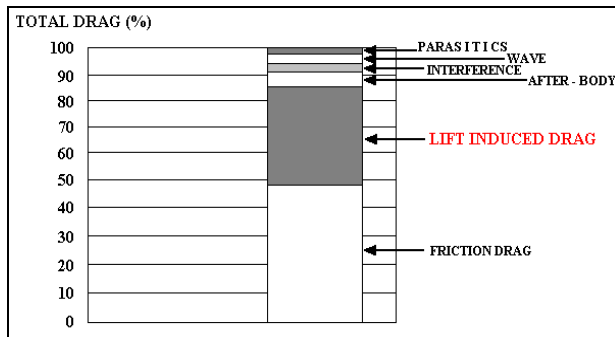


Fig. 1. Drag Breakdown of a Typical Transport Aircraft [1]

Finally, while wingspan extensions can reduce the drag of a given airplane, an increase in weight of the original wing is unavoidable. Additional weight penalties can also occur if the extension aggravates flutter for instance. The potential for drag savings has led to several new tip designs appearing on commercial aircraft [2].

1.1 Technical Discussion

Producing induced drag on a finite wing is accompanied by spanwise flow over the wing surface. In particular, the pressure gradients caused by the lower pressures on the upper surface relative to the higher pressures on the lower surface lead to inward spanwise flow on the upper surface and outward spanwise flow on the lower. At the trailing edge, the merging of these two flows with different directions generates a vorticity that is shed from the finite wing and is the origin of induced drag.

It has been known for over a century that an endplate at the tip of a finite wing can reduce the spanwise flow and thereby reducing the induced drag. Unfortunately, to be effective, the endplate must be so large that the increase in wetted area drag outweighs any drag reduction. A winglet carries an aerodynamic load which produces a flowfield interacting with that of the main wing thereby reducing the amount of spanwise flow rather than being a simple fence which limits the spanwise flow. In essence, the winglet diffuses the influence of the tip vortex so that the downwash and the induced drags are reduced. In this way, the winglet acts like an endplate in reducing the spanwise flow; however by carrying the proper aerodynamic

loading, this is accomplished with much less wetted area.

A different way of explanation is that the winglet produces a vertical diffusion of the vorticity in tip region. This diffusion process is also realized as an expansion of the wake in the far field due to the induced velocities from the non-planar components of the winglet. The out of plane bound vortex on the upward winglet induces horizontal velocities on the free wake that cause a spanwise spreading of the wake field [3].

2 Experimental Apparatus

Experiments were conducted in the low speed wind tunnel at Sharif University of Technology (SUT), department of Mechanical Engineering. The tunnel is an open circuit indraft with a rectangular test section of $45 \times 45 \times 160 \text{ cm}^3$. The maximum obtainable speed in the test section is approximately 45 m/sec. A half-span wing with sweep angle of 20 degrees is mounted in the test section. The angle of attack is varied manually from zero to 90 degrees. Figures 2 and 3 show the tunnel and the model as well as different winglet shapes used in this investigation.



Fig. 2. SUT wind tunnel

EXPERIMENTAL INVESTIGATION OF THE EFFECT OF VARIOUS WINGLET SHAPES ON THE TOTAL PRESSURE DISTRIBUTION BEHIND A WING



Fig. 3. The wing model including winglet shapes

Four types of winglet shapes, spiroid [4,5] (forward and aft), blended winglets [6], and winggrid [7,8] are used in this investigation. The wing model used in this study has an average chord of 15.7 cm made of fiberglass and manufactured using a numerically controlled milling machine. The Spiroid-typed winglets are made of aluminum and the remaining winglets are made of plexi-glass. Two types of spiroid winglets are used as shown in Figures 4 and 5, Forward (FWD) spiroid winglet and Aft (AFT) spiroid winglet.

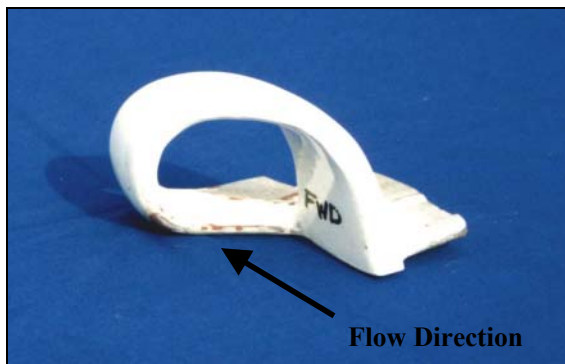


Fig. 4. FWD spiroid winglet model

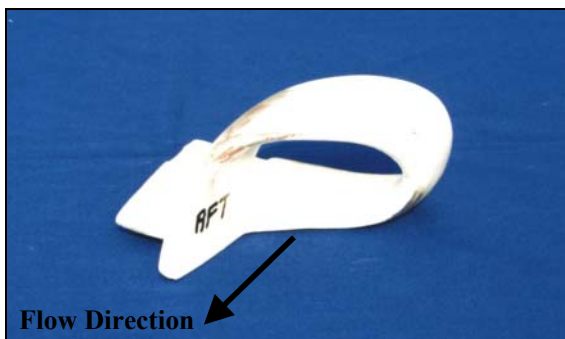


Fig. 5. AFT spiroid winglet model

A 32-tube rake probe is mounted horizontally from the back of the model. A traversing mechanism positions incrementally the probe across the wake. The probe is positioned at the tunnel centerline and the wake survey data are measured at a single traverse plane (at a distance of 2.0 times average chord) downstream of the model trailing edge. Both surface pressures and wake data are obtained using HCXPM010D6V and HCXPM005D6V pressure transducers with a quoted accuracy of 0.2% of full-scale pressure range. Each transducer data is collected via a multiplexer and transferred to the computer through a 16-bit Analog-to-Digital (A/D) board. Various sampling rates are performed and finally the best one is selected.

3 Results and Discussions

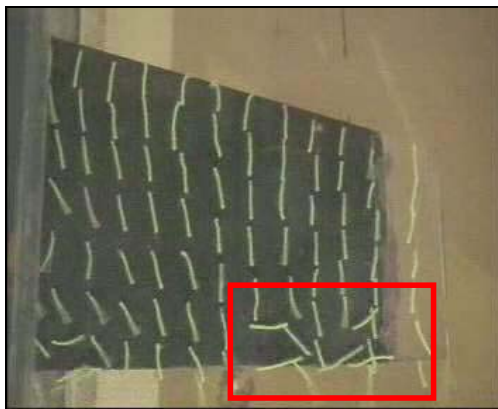
All measurements are conducted at a Reynolds number of 200000, using four different types of winglet at various angles of attack. The wake data for all winglets are measured. Each flowfield data set acquired in the tunnel (the traverse plane) comprised of approximately 2500 data points. Reduction of the raw pressure data yielded axial velocity component and total as well as static pressure coefficients. The repeatability of the pressure data from the winglet models is also analyzed. For further information the reader is referred to reference [9].

3.1 Flow Visualization

In order to recognize the wing flow pattern, tufts are used. Tufts are small, visible, and light threads attaching in well-positioned places over the wing so that the flow direction is clearly seen. Figures 6a–e show one of the positions of flow pattern being photographed. The angle of attack of the wing, for this case is 10 degrees. The flow direction over a typical swept and tapered wing on the upper surface is from tip to root, which is exactly the same as its stall pattern (Fig. 7.). The flow pattern over the model used in this investigation follows the same manner. The stall characteristic is supposed to be similar to those shown in Fig. 7., for the wing without winglet. However, for any kind of installed winglets, the

flow field will change drastically, thus changing the stall characteristics. It should be noted that not all winglets changed the flow field in the same way (Fig. 6.).

From this figure it is clearly seen that the flow direction near the tip of wing, as marked in the figure, differs for each winglet, while the angle of attack for all cases are the same. Inspections show that the tip vortex for the cases in Figures 6b and 6c are stronger than other cases and the flow is more complicated. As seen in Fig. 6b and c, the flow direction on the trailing edge (TE) of the wingtip is contrary to what is expected in Fig. 7. The flow direction normally on the upper surface of a swept wing is from tip to root; however, for the wing equipped with Spiroid winglet the opposite is true - that is, from root to tip. However, for the wing grid case, Fig. 6e, the tufts are not affected by the winglet significantly. For the bare wing one, Fig. 6a, it is seen that the flow is almost separated in the tip region.



(a) Bare Wing



(b) FWD Spiroid



(c) AFT Spiroid



(d) Blended



(e) Wing Grid

Fig. 6. Flow Visualization with Tufts, $\alpha=10^\circ$

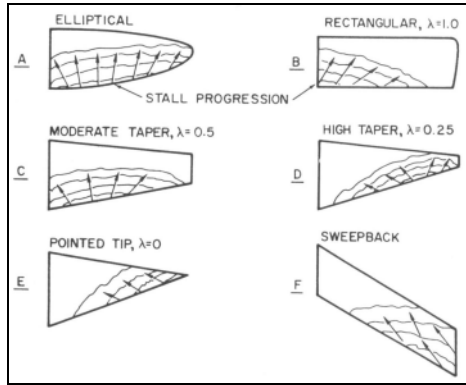


Fig. 7. Stall Patterns

3.2 Total Pressure Distribution

A 32-tube rake probe mounted horizontally from the back of the model measured the total pressure distribution behind the wing. The measurement nodes comprised of approximately 2500 data points, which form a grid shown in Fig. 8. Note that the total pressure distribution is measured in the wake of the model at a distance of $x/c=2$.

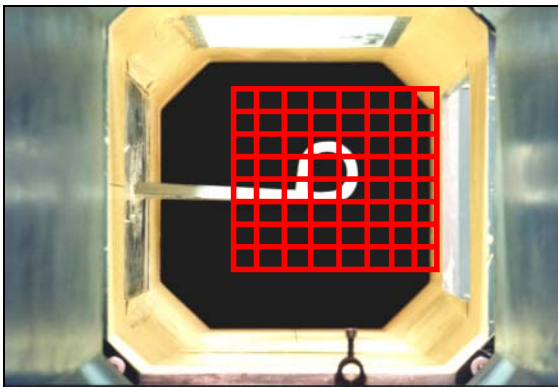
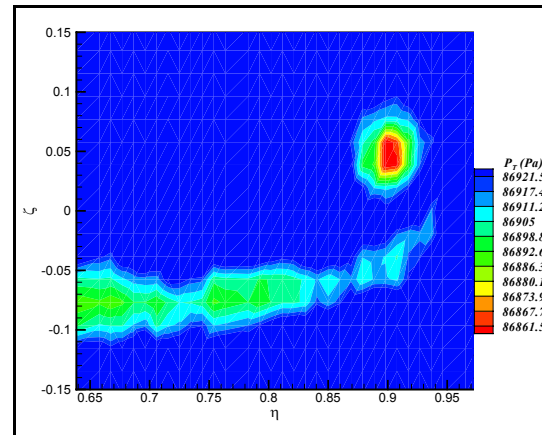


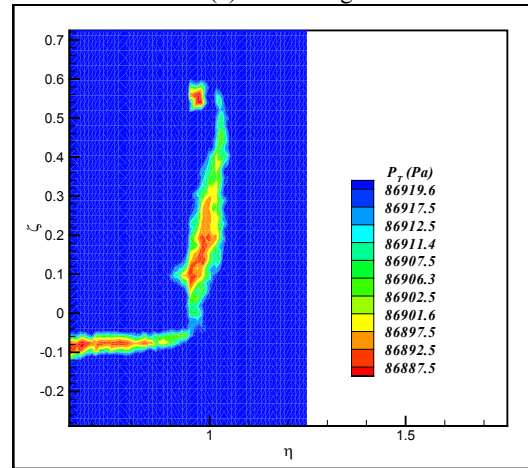
Fig. 8. Domain of total pressure measurements behind the wing

Figure 9.a-e. shows total pressure distribution behind the wing with four different winglets at zero angle of attack. The pressure distribution for the bare wing (wing without winglet) is also shown as comparison (Fig. 9.a). It can be seen by inspection that at zero angle of attack, the tip vortex for the bare wing is quite clear. The airfoil used in this wing is not symmetric, thus at zero angle of attack it produces some lift which is the result of different pressure distribution over its upper and lower surfaces. As a result of this lift, a tip vortex will be generated as seen by Fig.9.a. The tip vortices for the cases with winglet are different from that of the bare wing, Fig.9.b-e. From this

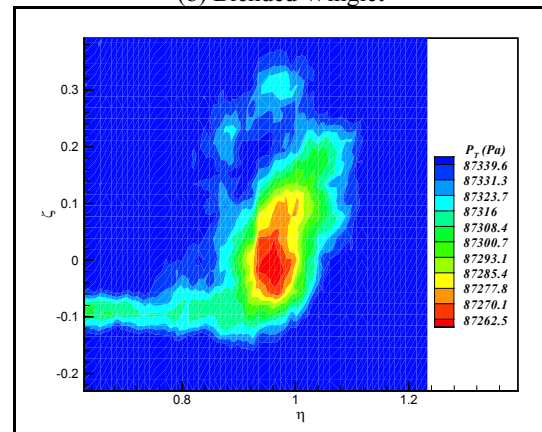
figure by inspection it is seen that for this angle of attack, the tip vortex for the blended winglet, Fig.9.b, is slightly weaker than other vortices. For other winglets, FWD spiroid, AFT spiroid, and winggrid one the shape and width of the tip vortex differs significantly from those of the bare and blended ones.



(a) Bare Wing



(b) Blended Winglet



(c) FWD Spiroid

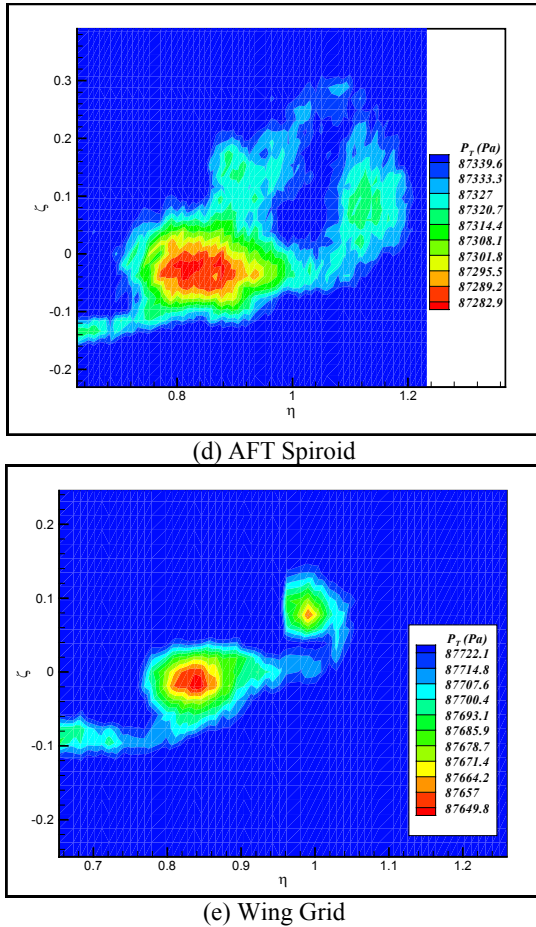


Fig. 9. Effect of different winglet shapes on total pressure distribution behind the wing, $\alpha=0^\circ$

Effects of angle of attack on the tip vortices formed by those winglets are shown in figures 10 and 11. Again the data for the bare wing are shown for both angle of attack, $\alpha=10^\circ$, 15° for comparison. As the angle of attack increases, the height, width, and strength of the tip vortices varies significantly, figures 10.a and 11.a. As seen from this figure, the tip vortex for the clean model moves inward (toward the root) and the vortex core widens, figures 10.a and 11.a.

Figure 10.a shows that the maximum height of the tip vortex core for the clean model at $\alpha=10^\circ$ is about $\zeta \approx 0$, while for the other two cases shown in Figures 10.c and 10.d, and for the same angle of attack, $\zeta=0$ and $\zeta=0.12$, respectively. Further comparing Figures 10.c and 10.d, it is clear that the FWD spiroid winglet displaces the wake upward, i.e. above the primary tip vortex, while the AFT spiroid

case moves the wake below the primary tip vortex. The wake formation behind these two winglets, FWD spiroid and the AFT one as seen from Figure 10, differs from each other significantly. More experiments are needed to better understand these phenomena.

The effect of Blended winglet on the total pressure distribution in the wake of the model measured at $x/c=2.0$ and $\alpha=10^\circ$ is shown in Figure 10.b. From this figure two relatively weak tip vortices are seen. The total pressure loss caused by these vortices in the wake of the model is again less than that of the bare wing, shown in Figure 10.a. Also, comparing Figures 10.a and 10.b, it could be seen that the height of the tip vortex of the bare wing is lower than that of the blended one. The blended winglet creates two tip vortices, one reaches maximum height of about $\zeta=0.05$ and the second one reaches $\zeta=0.45$. While the maximum height of the core of the tip vortex for the bare wing is near $\zeta=0$, Figure 10.a. Further, it should be mentioned that the first tip vortex of the blended winglet is much weaker than that of the bare wing, Figure 10.a.

Comparing Figure 10.a and Figure 10.b, it seems likely that for both cases, the primary tip vortices have almost the same height, $\zeta \approx 0$, although the blended winglet has displaced the primary tip vortex slightly, Figure 10.b. However, the blended winglet has created another vortex that is located at a height of about $\zeta=0.45$. This vortex is probably due to the blended winglet itself, which acts as a half model wing attached at one end to the primary model tip instead of the tunnel wall. Thus it seems likely that this winglet will generate a tip vortex itself when the flow passes over it. However, for the spiroid cases shown in Figure 10, the situation is different. Also note that both ζ and η for the tip vortex of the bare wing are much larger than those of the blended winglet ones, i.e. the bare wing has a much larger tip vortex. Further comparing Figures 10.c and 10.d with Figure 10.b, it is clearly seen that the width of the wake generated by the blended winglet is much smaller than those of spiroid ones. Note that all cases shown here are for the same angle

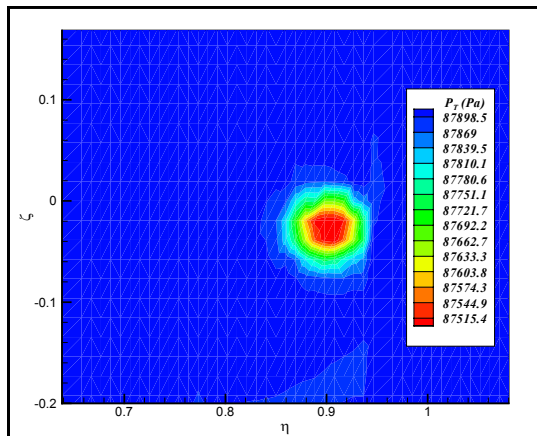
EXPERIMENTAL INVESTIGATION OF THE EFFECT OF VARIOUS WINGLET SHAPES ON THE TOTAL PRESSURE DISTRIBUTION BEHIND A WING

of attack and the measured total pressure are at the same distance behind the model, $x/c=2.0$.

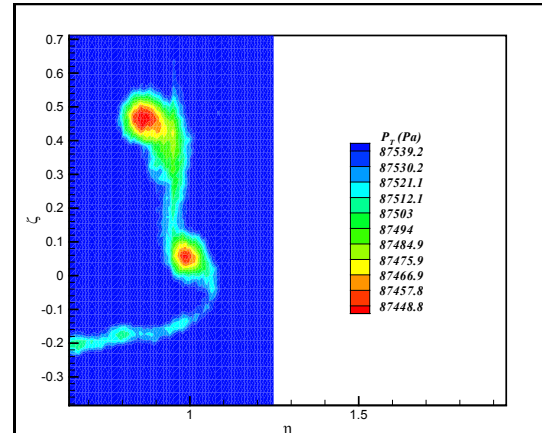
Figure 10.e shows total wake pressure distribution at $x/c=2.0$ behind the model equipped with the winggrid. Although the tip vortex formed by this winglet is similar to that of the bare wing one, Figure 10.a, the wake behind the model is different. Further it seems that this type of winglet has displaced the tip vortex too, $\zeta=0.05$. Note for the bare wing case, when at the same condition, the height of the vortex core was about $\zeta \approx 0$. Other data at different angles of attack show similar trends [10].

For higher angle of attack, $\alpha=15^\circ$, Fig.11, the shape of vortices formed behind the wing equipped with winglets vary significantly with the corresponding ones but at lower alpha, Fig.10. It is seen by inspection that the main vortex formed by the blended winglet is widened and has moved inward, Fig.11.b. However, the second vortex formed by this winglet, due to the winglet itself, is much weaker than that of figure.10.b. Furthermore, comparing figure.11.c and 10.c, it is seen that the changes in the tip vortex of the FWD spiroid is much less than that of the AFT one, Fig.11.d and 10.d.

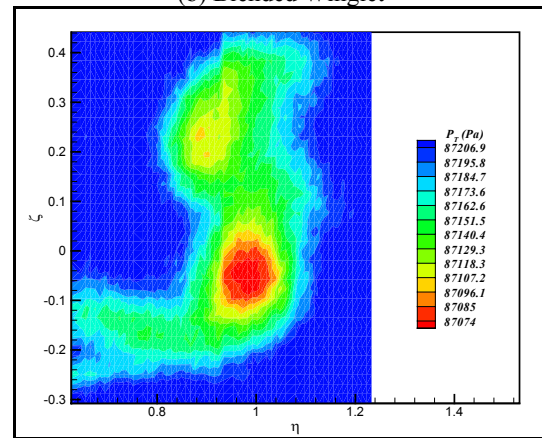
The flowfield behind the wing equipped with winggrid also shows some variations with angle of attack. As alpha increases, the tip vortex moves toward the wing root and shifts downward slightly, Fig.11.e and 10.e.



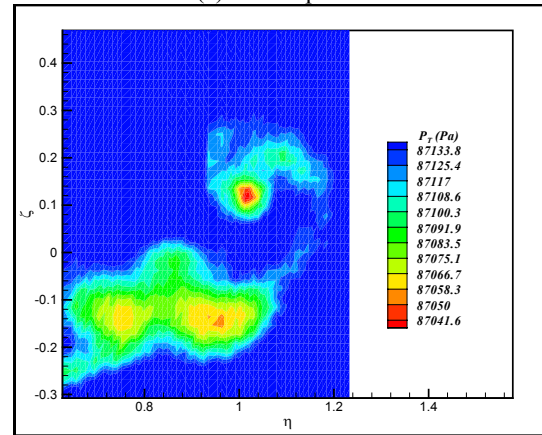
(a) Bare Wing



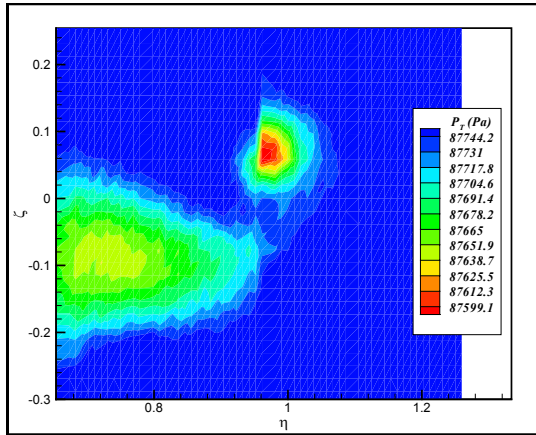
(b) Blended Winglet



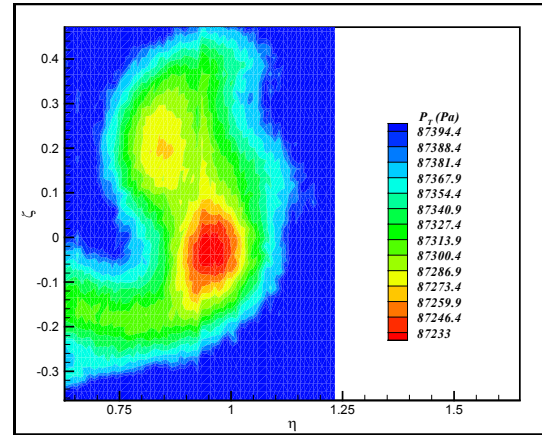
(c) FWD Spiroid



(d) AFT Spiroid

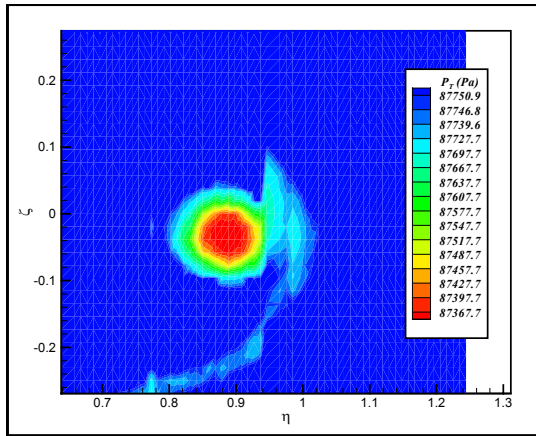


(e) Wing Grid

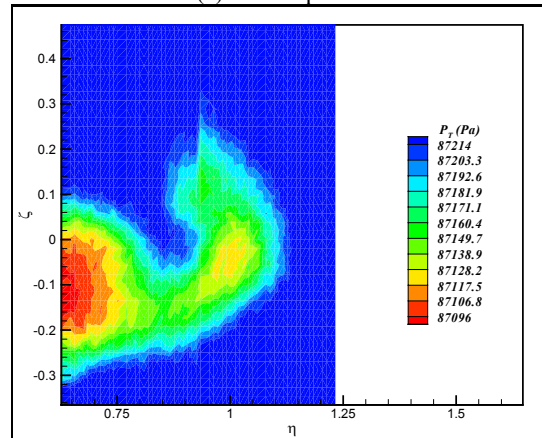


(c) FWD Spiroid

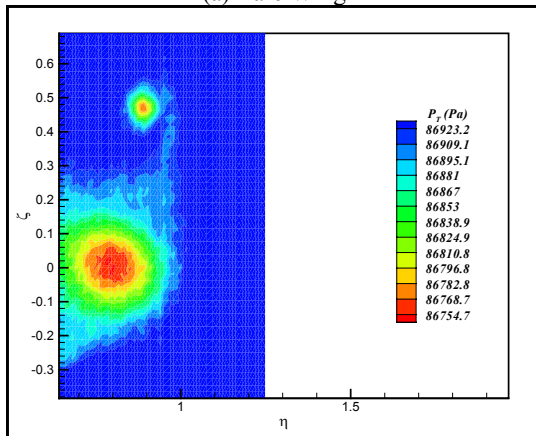
Fig. 10. Effect of different winglet shapes on total pressure distribution behind the wing, $\alpha=10^\circ$



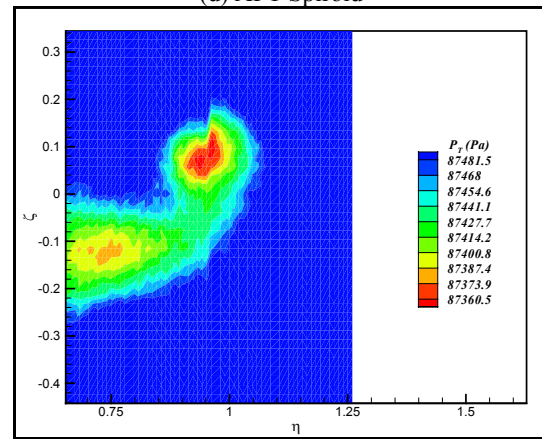
(a) Bare Wing



(d) AFT Spiroid



(b) Blended Winglet



(e) Wing Grid

Fig. 11. Effect of different winglet shapes on total pressure distribution behind the wing, $\alpha=15^\circ$

EXPERIMENTAL INVESTIGATION OF THE EFFECT OF VARIOUS WINGLET SHAPES ON THE TOTAL PRESSURE DISTRIBUTION BEHIND A WING

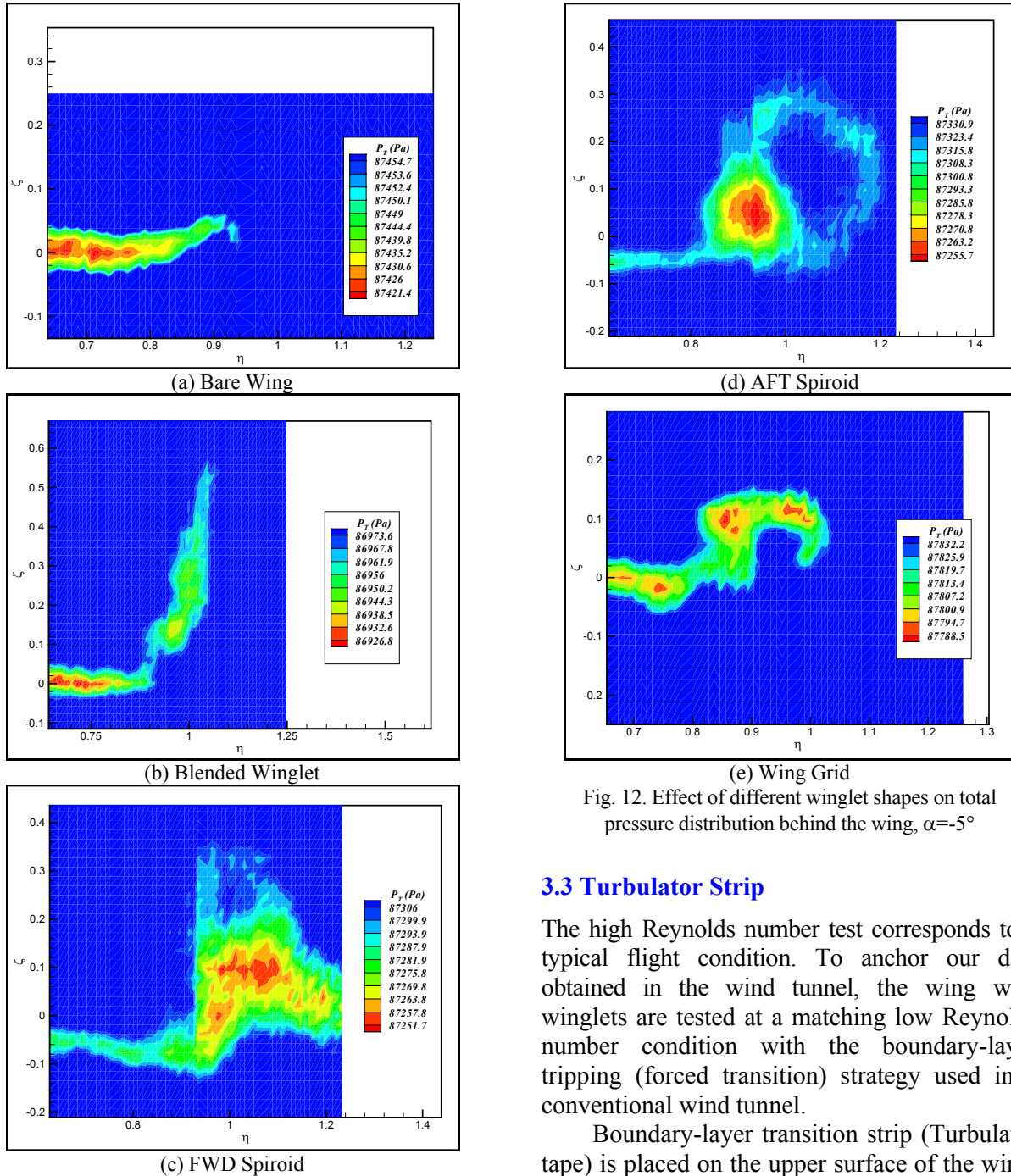


Fig. 12. Effect of different winglet shapes on total pressure distribution behind the wing, $\alpha = -5^\circ$

3.3 Turbulator Strip

The high Reynolds number test corresponds to a typical flight condition. To anchor our data obtained in the wind tunnel, the wing with winglets are tested at a matching low Reynolds number condition with the boundary-layer tripping (forced transition) strategy used in a conventional wind tunnel.

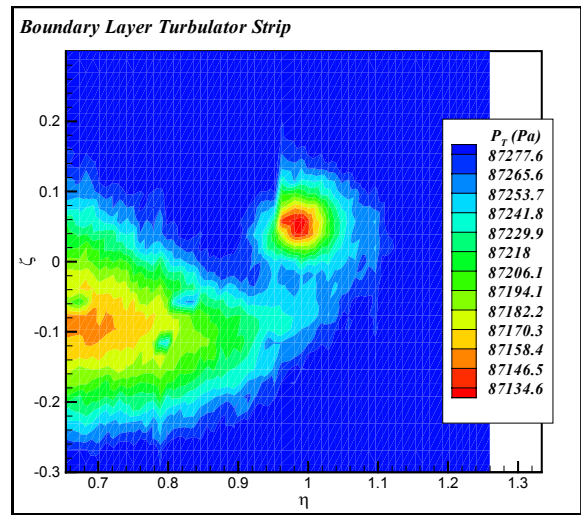
Boundary-layer transition strip (Turbulator tape) is placed on the upper surface of the wing. The turbulator strip consists of a 0.5 cm wide band of sandpaper grains set in a plastic adhesive. The turbulator tape is applied at 10% average chord from the wing leading edge [11].

In order to demonstrate that the flow over 90% of the aft chord of the wing model is changed to turbulent, the Eppeler Analysis Code [12] is used to calculate the transition point. The

transition point was calculated to be located at about 10% of the average chord from LE.

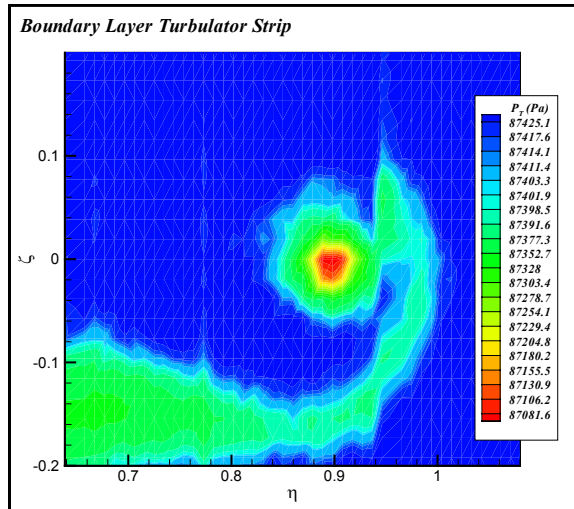
Figure 13. shows variation of total pressure behind the bare wing and wing with winggrid at $\alpha=10^\circ$. For both cases shown in this figure the model is equipped with turbulator strip installed at $x/c=0.1$, hence creating early flow transition.

Comparing the total pressure distribution over the wing surface for this case, figure 13, with the corresponding ones but without turbulator, Fig. 10.a and 10.e, it is seen that the turbulator has not changed the shape and orientation of the vortices significantly. However, the wake behind the model with turbulator is slightly thickened and the total pressure has been reduce, figure 13. Surface pressure data [10] shows similar trend and indicates that the transition has occurred at a place where the turbulator is installed. The total pressure reduction is due to the change of the laminar flow to turbulent, while the difference in flow regime has only quantitative effect.



(b) Wing Grid

Fig. 13. Effect of Turbulator strip on the wing total pressure distribution, $\alpha=10^\circ$



(a) Bare Wing

4 Conclusions

The effect of different winglet shapes on the flowfield behind a tapered wing has been experimentally investigated. The measurement included total wake survey behind the wing at various angles of attack with different winglet shapes, flow visualization over the wing surface using tufts, etc. The effect of Reynolds number was investigated by forcing flow transition over the model surface at about $x/c \approx 0.1$.

The total pressure data in the wake show significant changes for different winglets, but at the same angle of attack. The tip vortices formed by different winglet shapes are totally different from each other and seen that they may have significant effect on the flowfield over the wing surface. These vortices vary differently while the model angle of attack changes. The value of the total pressure measured behind these winglets differs from each other too, indicating their effect on the induced drag. Furthermore, winglets displaced the primary tip vortex and changed its sharp in comparison with that of the bare model. However, these variations differ for each winglet; i.e. different winglets changed the abovementioned characteristics differently. More detailed experimental as well as computational investigations are needed to better understand these phenomena and their effect on the

overall force and moments generated by the wing when equipped with different winglets.

5 Acknowledgments

The present work has been funded in part by the Institute for Aeronautical Research, Bureau of Aircraft Design, HESA. The authors would like to thank the Director of the Design Bureau for his support.

References

- [1] Thiede, P., (Editor), *Aerodynamic Drag Reduction Technologies*. Proceedings of the CEAS/DragNet European Drag Reduction Conference, 19-21 June 2000, Potsdam, Germany, 1st Ed., Springer, 2001.
- [2] Gold, N. and Visser, K.D. Aerodynamic Effects of Local Dihedral on a Raked Wingtip. *40th AIAA Aerospace Sciences Meeting & Exhibit*, Reno, NV, AIAA-2002-0831, January 14-17, 2002.
- [3] Maughmer Mark D. The Design of Winglets for High-Performance Sailplanes. *AIAA-2001-2406*, 2001.
- [4] Gratzler, Louis, B. Spiroid-Tipped Wing. *United States Patent # 5,102,068*, April 7, 1992.
- [5] The Spiroid-Tipped Wing. 2001, available on-line; URL:
<http://www.aviationpartners.com/company/concepts.html>
- [6] Gratzler, Louis, B. Blended Winglet. *United States Patent # 5,348,253*, September 20, 1994.
- [7] La Roche. Wing With a Wing Grid As The End Section. *United States Patent # 5,823,480*, October 20, 1998.
- [8] La Roche et al. Wing Comprising a Distal Wing Grid. *United States Patent # 6,431,499, B1*, August 13, 2002.
- [9] Nazarinia, M. *Flow Analysis Over and Behind a Wing with Different Winglets*. M.Sc. Thesis, Sharif University of Technology, Department of Aerospace Engineering, 2003.
- [10] Soltani M.R., Ghorbanian K. and Nazarinia M. Flow Analysis Over and Behind a Wing with Different Winglet Shapes. *42nd Aerospace Sciences Meeting & Exhibit*, Reno, NV, AIAA 2004-0723, January 4-8 2004.
- [11] Albert E. von Doenhoff; Elmer A. Horton. A Low-Speed Experimental Investigation of the Effect of a Sandpaper Type of Roughness on Boundary-Layer Transition. *NACA Report 1349*, 1956, (Supersedes NACA Technical Note 3858).
- [12] Eppler; Richard. *Airfoil Design and Data*, Springer-Verlag, 1990.